mathematics

MDPI

Article

Impact of Variable Fluid Properties and Double Diffusive Cattaneo–Christov Model on Dissipative Non-Newtonian Fluid Flow Due to a Stretching Sheet

Khalil M. Khalil [1], A. Soleiman [1] and Ahmed M. Megahed [2,*] and W. Abbas [3]

[1] Department of Mathematics, College of Science and Arts—Gurayat, Jouf University, Sakakah 77454, Saudi Arabia; kmshalaby@ju.edu.sa (K.M.K.); asoliman@ju.edu.sa (A.S.)
[2] Department of Mathematics, Faculty of Science, Benha University, Benha 13518, Egypt
[3] Basic and Applied Science Department, College of Engineering and Technology, Arab Academy for Science, Technology and Maritime Transport, Cairo 11511, Egypt; wael_abass@aast.edu
* Correspondence: ahmed.abdelbaqk@fsc.bu.edu.eg

Abstract: The present work focuses on the attributes of flow, heat, and mass transfer together with double diffusive Cattaneo–Christov mechanism with regards to their applications. The aim of this study is to investigate the non-Newtonian Powell–Eyring fluid flow, taking into account the twofold impact of the heat generation mechanism and the viscous dissipation due to an extensible sheet. The chemical reaction between the fluid particles and the fluid variable properties is assumed in this study. The motive behind this study is the continuous and great interest in the utilization of non-Newtonian liquids in organic and technical disciplines. This model is administered and governed by the momentum equation, energy equation, and concentration, all of which are in the form of partial differential equations. With the help of the shooting technique, the numerical solution is obtained. Graphs show the characteristics of flow, heat, and mass transfer mechanisms for various governing parameters. Additionally, significant physical non-dimensional quantities have been presented in a tabular form. The outcomes detect that increasing the Deborah number, which is connected with the mass transfer field and the chemical reaction parameter, decreases the concentration distribution.

Keywords: Cattaneo–Christov model; Powell–Eyring fluid; chemical reaction; variable fluid properties

Citation: Khalil, K.M.; Soleiman, A.; Megahed, A.M.; Abbas, W. Impact of Variable Fluid Properties and Double Diffusive Cattaneo–Christov Model on Dissipative Non-Newtonian Fluid Flow Due to a Stretching Sheet. *Mathematics* **2022**, *10*, 1179. https://doi.org/10.3390/math10071179

Academic Editor: James M. Buick

Received: 12 March 2022
Accepted: 1 April 2022
Published: 5 April 2022

1. Introduction

With the rapid progress of engineering design innovations, the non-Newtonian fluid as a new material has gained substantial attention. This wide interest is owing to their importance in numerous industrial applications, such as modern technology, transportation, biomedicine, and electronics. Important applications also include the expulsion of elastic sheets, veins, water system channels and the cooling of continuous strips, etc. Because of these diverse and novel technological and innovative applications for non-Newtonian models, many researchers have looked into this topic and its various applications. For example, a non-Newtonian micropolar type was presented by Haliza et al. [1], with further subtleties on the topic of non-Newtonian Maxwell fluids able to be viewed in [2–4], while the non-Newtonian Casson fluid has been evaluated under the impact of slip phenomena by Imran et al. [5]. On the same topic, Sharma et al. [6] explored the non-Newtonian Casson–Williamson fluid flow over a stretched sheet of non-uniform thickness, whereas Muhammad and Samia [7] investigated the non-Newtonian Powell–Eyring fluid due to a stratified sheet with mixed convection. Similarly, Megahed and Abbas [8] studied non-Newtonian cross fluid under the impact of the thermal stratification phenomenon.

The investigations listed above are limited to traditional heat and mass transfer models that are controlled by Fourier laws. The characteristics of heat transfer can be determined precisely if we consider the fact that the relaxation time for velocity fields must occur during

the fluid flow. The relaxation time phenomenon that influences both the concentration and the temperature fields is governed by the Cattaneo–Christov model [9]. Nowadays, the Cattaneo–Christov heat motion model is a type of Fourier law amended by fusing the relaxation time term with the spread of heat flux through the physical model [10]. Hayat et al. [11] explored the impact of variable conductivity on the non-Newtonian Jeffrey fluid with the Cattaneo–Christov model and variable thickness. Cattaneo–Christov double diffusion influence in the non-Newtonian Walters-B nanofluid has been investigated by Hayat et al. [12]. The Cattaneo–Christov model was further scrutinized by Sui et al. [13] for Maxwell nanofluids with a slip velocity phenomenon, by Shehzad et al. [14] for third-grade fluid flow, by Li et al. [15] for a viscoelastic fluid model under the effect of the magnetic field, by Meraj et al. [16] for a Jeffrey fluid model together with Darcy–Forchheimer flow, and by Shehzad et al. [17] for chemically non-Newtonian Maxwell liquid with 3D hydromagnetic flow. Subsequent studies regarding the topic of the Cattaneo–Christov model are introduced in Refs. [18–21]. The shooting method was used in most prior studies, as it is in this one, although there are a variety of different numerical approaches that can be used to solve the Navier–Stokes equations, which have been studied in Refs. [22,23].

The previously mentioned examinations reveal that a lot of investigations might be cited regarding the matter of Cattaneo–Christov through different types of non-Newtonian fluid. In any case, fewer studies are considered through the literature review that imply the combination of the Cattaneo–Christov model and the non-Newtonian Powell–Eyring fluid. Yet, no review has talked about the Cattaneo–Christov heat flux model on a dissipative non-Newtonian Powell–Eyring fluid with variable fluid properties and a chemical reaction mechanism. The creativity of the displayed problem is enhanced with the extra effects of the heat generation mechanism and the viscous dissipation phenomenon. The current study is performed with the assumption of the fluid flow due to the linear stretching of an elastic sheet. Finally, we adopted a shooting procedure to deal with such a physical problem.

2. Fundamental Governing Equations

Herein, we will consider consistent two-dimensional laminar Powell–Eyring fluid flow and heat mass transfer together with the Cattaneo–Christov phenomenon. This type of non-Newtonian fluid can be evermore characterized by the parameters β and c. The fluid velocity components are assumed to be symbolized by u and v in $x-$ and $y-$ directions, respectively (Figure 1). The fluid particles are likewise assumed to chemically react together with their gaining warmth due to the presence of the heat generation source. It is also presumed that the sheet has a constant temperature T_{w} and it is extended with speed $u_{\mathrm{w}} = ax$.

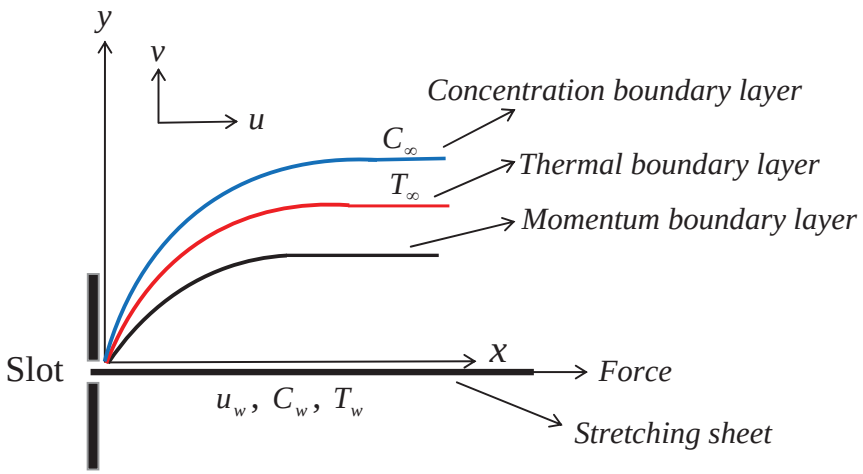

Figure 1. Physical configuration.

Furthermore, the impact of the viscous dissipation on the heat transfer mechanism through the thermal boundary layer is taken into account. Considering the above physical assumptions, the administering equations for the Powell–Eyring model can be introduced as follows [24]:

$$\frac{\partial u}{\partial x}+\frac{\partial v}{\partial y}=0, \tag{1}$$

$$u\frac{\partial u}{\partial x}+v\frac{\partial u}{\partial y}=\frac{1}{\rho_\infty}\frac{\partial}{\partial y}\left(\mu\frac{\partial u}{\partial y}+\frac{1}{\beta c}\frac{\partial u}{\partial y}-\frac{1}{6\beta c^3}(\frac{\partial u}{\partial y})^3\right), \tag{2}$$

$$\begin{aligned}u\frac{\partial T}{\partial x}+v\frac{\partial T}{\partial y}+\lambda_1\Phi_E=\frac{1}{\rho_\infty c_p}\frac{\partial}{\partial y}\left(\kappa\frac{\partial T}{\partial y}\right)+\frac{Q}{\rho_\infty c_p}(T-T_\infty)\\ +\frac{1}{\rho_\infty c_p}\left(\mu(\frac{\partial u}{\partial y})^2+\frac{1}{\beta c}(\frac{\partial u}{\partial y})^2-\frac{1}{6\beta c^3}(\frac{\partial u}{\partial y})^4\right)\end{aligned} \tag{3}$$

$$u\frac{\partial C}{\partial x}+v\frac{\partial C}{\partial y}+\lambda_2\Phi_C=D\frac{\partial^2 C}{\partial y^2}-k_0(C-C_\infty). \tag{4}$$

The fluid flow is exposed to the following boundary conditions:

$$u=u_\mathrm{w}=ax,\quad v=0,\quad T=T_\mathrm{w},\quad C=C_\mathrm{w}\quad \text{at}\quad y=0, \tag{5}$$

$$u\to 0,\quad T\to T_\infty,\quad C\to C_\infty,\quad \text{at}\quad y\to\infty, \tag{6}$$

where

$$\Phi_E=u\frac{\partial u}{\partial x}\frac{\partial T}{\partial x}+v\frac{\partial v}{\partial y}\frac{\partial T}{\partial y}+u\frac{\partial v}{\partial x}\frac{\partial T}{\partial y}+v\frac{\partial u}{\partial y}\frac{\partial T}{\partial x}+2uv\frac{\partial^2 T}{\partial x\partial y}+u^2\frac{\partial^2 T}{\partial x^2}+v^2\frac{\partial^2 T}{\partial y^2}, \tag{7}$$

$$\Phi_C=u\frac{\partial u}{\partial x}\frac{\partial C}{\partial x}+v\frac{\partial v}{\partial y}\frac{\partial C}{\partial y}+u\frac{\partial v}{\partial x}\frac{\partial C}{\partial y}+v\frac{\partial u}{\partial y}\frac{\partial C}{\partial x}+2uv\frac{\partial^2 C}{\partial x\partial y}+u^2\frac{\partial^2 C}{\partial x^2}+v^2\frac{\partial^2 C}{\partial y^2}. \tag{8}$$

where κ is the fluid thermal conductivity, ρ_∞ is the ambient density, μ is the Powell–Eyring viscosity, T is the fluid temperature, C is the fluid concentration, T_w is the sheet temperature, C_w is the sheet concentration, T_∞ is the encompassing fluid temperature, C_∞ is the encompassing fluid concentration, k_0 is the rate of chemical reaction, λ_1 is the relaxation time for the heat flux, D is the coefficient of diffusion, λ_2 is the relaxation time for the mass flux and Q is the coefficient of heat generation (absorption).

In light of Equations (1)–(4), pick the following proper dimensionless transformations as:

$$u=axf'(\eta),\quad v=-\sqrt{a\nu_\infty}f(\eta),\quad \eta=y\sqrt{\frac{a}{\nu_\infty}},\quad \theta(\eta)=\frac{T-T_\infty}{T_\mathrm{w}-T_\infty},\quad \phi(\eta)=\frac{C-C_\infty}{C_\mathrm{w}-C_\infty}. \tag{9}$$

Considering that the liquid conductivity and the liquid viscosity modifies with temperature as indicated by the accompanying relations [25]:

$$\mu=\mu_\infty e^{-\gamma\theta}, \tag{10}$$

$$\kappa=\kappa_\infty(1+\varepsilon\theta), \tag{11}$$

where μ_∞ is the viscosity of the Powell–Eyring fluid at the ambient, γ is the viscosity parameter, κ_∞ is the liquid thermal conductivity at the surrounding and ε is the thermal conductivity parameter. Now, considering the last supposition for both the liquid viscosity and the liquid conductivity, Equation (1) is consequentially fulfilled while the remaining equations reduce to the following system:

$$f'''\left(e^{-\gamma\theta}+\alpha(1-\delta f''^2)\right)-\gamma f''\theta' e^{-\gamma\theta}-f'^2+ff''=0, \tag{12}$$

$$\frac{1}{Pr}\Big((1+\varepsilon\theta)\theta'' + \varepsilon\theta'^2\Big) + f\theta' - De_1\Big(ff'\theta' + f^2\theta''\Big) + \beta_1\theta + Ecf''^2\left((e^{-\gamma\theta}+\alpha) - \frac{\alpha\delta}{3}f''^2\right) = 0 \tag{13}$$

$$\phi'' + Scf\phi' - ScDe_2\Big(ff'\phi' + f^2\phi''\Big) - Sc\xi\phi = 0. \tag{14}$$

Additionally, after invoking the previous dimensionless variables, the related physical boundary conditions are transformed as

$$f = 0, \quad f' = 1, \quad \theta = 1, \quad \phi = 1 \quad \text{at} \quad \eta = 0, \tag{15}$$

$$f' \to 0, \quad \theta \to 0, \quad \phi \to 0 \quad \text{at} \quad \eta \to \infty, \tag{16}$$

The arisen dimensionless governing parameters are the Powell–Eyring parameters α, δ, the thermal Deborah number De_1, the Eckert number Ec, the Prandtl number Pr, the heat generation (absorption) parameter β_1, the Deborah number which related to the mass transfer field De_2 and the chemical reaction parameter ξ which can be characterized as follows:

$$\alpha = \frac{1}{\mu_\infty \beta c}, \quad \delta = \frac{a u_w^2 \rho_\infty}{2c^2\mu_\infty}, \quad De_1 = \lambda_1 a, \quad Ec = \frac{u_w^2}{c_p(T_w - T_\infty)}, \tag{17}$$

$$Pr = \frac{\mu_\infty c_p}{\kappa_\infty}, \quad \beta_1 = \frac{Q}{a\rho c_p}, \quad De_2 = \lambda_2 a, \quad \xi = \frac{k_0}{a}. \tag{18}$$

Moreover, as indicated by the previous dimensionless variables in Equation (9), the local skin friction Cf_x, local Nusselt number Nu_x and local Sherwood number Sh_x are introduced as follows:

$$Cf_x Re^{\frac{1}{2}} = -\left((e^{-\gamma\theta(0)}+\alpha)f''(0) - \frac{\alpha\delta}{3}f'''(0)\right), \quad Nu_x Re^{\frac{-1}{2}} = -\theta'(0), \quad Sh_x Re^{\frac{-1}{2}} = -\phi'(0) \tag{19}$$

where $Re = \frac{u_w x}{\nu_\infty}$ is the local Reynolds number.

3. Solution Approach

The goal of this part is to use the numerical method known as the shooting method to come up with numerical solutions to our problem. In terms of ordinary differential equations, this method can be used to solve the initial value problem. This method's technique entails converting the governing system of ordinary differential Equations (12)–(14) into a new first-order system. The resulting system is numerically integrated with the updated boundary conditions using the Runge–Kutta (RK) technique, which incorporates a shooting scheme. The most notable characteristic of the present method is the selection of appropriate finite values of $\eta \to \infty$. To obtain $f''(0), \theta'(0)$ and $\phi'(0)$ for the mentioned boundary value problem, we use some initial guessed values on a specified set of miscellaneous parameters. This approach instantly turns the previously governing equations into the following equations:

$$W_1 = f(\eta), \quad W_1' = W_2, \quad W_2' = W_3, \tag{20}$$

$$W_3' = \frac{\gamma W_3 W_5 e^{-\gamma W_4} + W_2^2 - W_1 W_3}{e^{-\gamma W_4} + \alpha(1 - \delta W_3^2)}, \tag{21}$$

$$W_4 = \theta(\eta), \quad W_4' = W_5, \tag{22}$$

$$W_5' = \frac{De_1\Big(W_1 W_2 W_5 + W_1^2 W_5'\Big) - W_5(W_1 + \frac{\varepsilon}{Pr}) - \beta_1 W_4 - Ec((e^{-\alpha W_4}+\alpha)W_3^2 - \frac{\alpha\delta}{3}W_3^4)}{\frac{1}{Pr}(1+\varepsilon W_4)} \tag{23}$$

$$W_6 = \phi(\eta), \quad W_6^{'} = W_7, \tag{24}$$

$$W_7^{'} = ScDe_2(W_1W_2W_7 + W_1^2W_7^{'}) - ScW_1W_7 + Sc\xi W_6. \tag{25}$$

The boundary conditions are now as follows:

$$W_1(0) = 0, \quad W_2(0) = 1, \quad W_4(0) = 1, \quad W_6(0) = 1, \tag{26}$$

$$W_3(0) = \epsilon_1, \quad W_5(0) = \epsilon_2, \quad W_7(0) = \epsilon_3, \tag{27}$$

where ϵ_1, ϵ_2 and ϵ_3 are determined using Newton's methodology so that the outer boundary conditions $W_2(\infty), W_4(\infty)$ and $W_6(\infty)$ are fulfilled. To obtain the required solution, we employ the traditional RK technique to integrate the generated ODEs with the specified set of parameters. Finally, to meet the convergence condition, the process is repeated until the results are precise to the anticipated level of 10^{-7} accuracy.

4. Verification of Numerical Methodology

The motivation behind this segment is to prove the effectiveness and trustworthiness of the numerical results obtained via the shooting technique. For this reason, Table 1 is set up below as an examination between our results and the recently published work by Javed et al. [26]. The viscosity parameter was disregarded $\gamma = 0$, but both Powell–Eyring parameters α and δ were changed to see how they affected the local skin friction coefficient $Cf_xRe^{\frac{1}{2}}$. By alluding to this table, the validity and unwavering quality of all the numerical results of this exploration are confirmed.

Table 1. Comparison of $Cf_xRe^{\frac{1}{2}}$ with the results of Javed et al. [26] when $\gamma = 0$.

α	δ	Javed et al. [26]	Present Work
0.0	0.0	1.0000	1.0000000000
0.2	0.0	1.0954	1.0953998521
0.4	0.0	1.1832	1.1831852914
0.2	0.0	1.0954	1.0953998521
0.2	0.1	1.0940	1.0940001201
0.2	0.2	1.0924	1.0923898767

5. Outcomes with Discussion

This section intends to investigate the impact of the current problem's parameters on the momentum, temperature, and concentration of the non-Newtonian Powell–Eyring fluid through the following graphical representations. To this end, some figures are created by varying the value of a parameter within a specified range, while the others are rigidly assigned, such as $\delta = 0.3, \gamma = 0.2, \alpha = 0.3, De_1 = 0.2, \beta_1 = 0.1, \varepsilon = 0.2, Sc = 0.7, De_2 = 0.2, Ec = 0.2, \xi = 0.2$ and $Pr = 1.5$. Figure 2 shows the impact of the α parameter on the velocity field $f'(\eta)$, temperature field $\theta(\eta)$ and the concentration field $\phi(\eta)$. The ascent in the value of this parameter causes an upgrade in the speed field $f'(\eta)$, although the converse pattern is noticed for both the temperature $\theta(\eta)$ and the concentration field $\phi(\eta)$. Physically, the stimulation effect occurs as the α parameter increases, causing the fluid velocity to increase while the concentration and temperature distributions decrease.

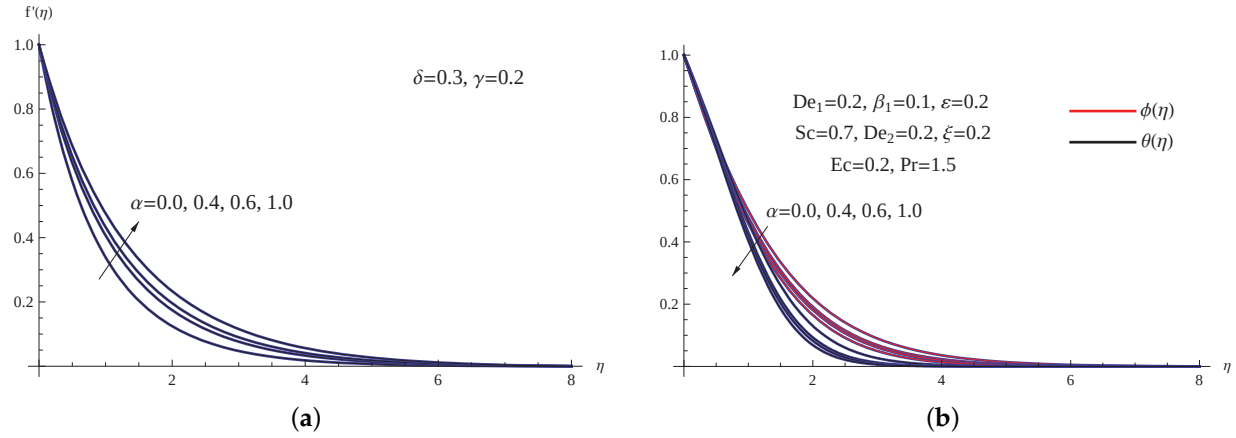

Figure 2. (**a**) $f'(\eta)$ for picked α. (**b**) $\theta(\eta)$ and $\phi(\eta)$ for picked α.

The impact of the δ parameter on the velocity profile, temperature profile, and concentration profile is shown in Figure 3. The heightening values of the δ parameter slightly improve both the temperature $\theta(\eta)$ and the concentration fields $\phi(\eta)$, whereas the opposite with the same marginal effect is noticed for the velocity field $f'(\eta)$. The Powell–Eyring parameter δ is physically dependent on the fluid density. As a result, as the Powell–Eyring parameter δ is increased, the density of the fluid particle increases, and the velocity profile decreases.

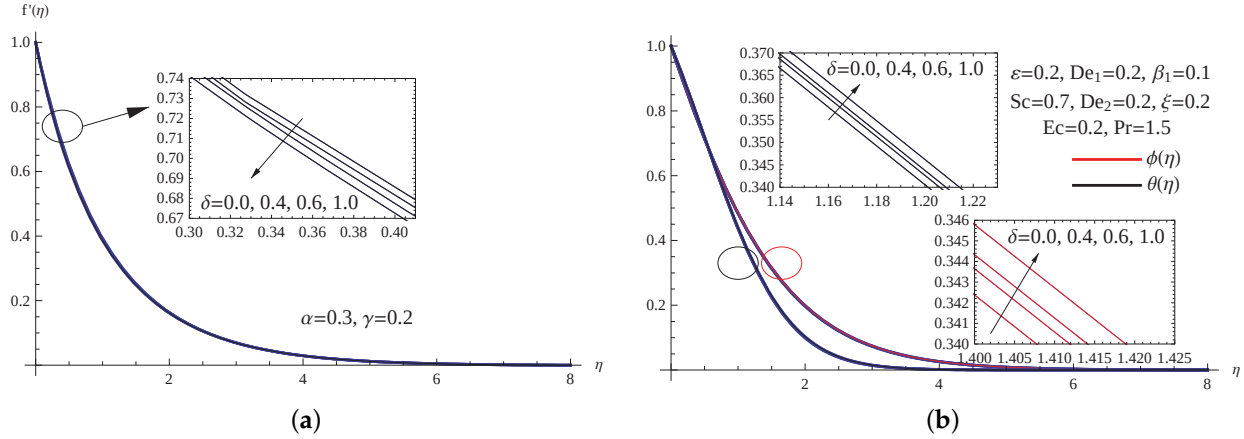

Figure 3. (**a**) $f'(\eta)$ for picked δ. (**b**) $\theta(\eta)$ and $\phi(\eta)$ for picked δ.

Figure 4 is plotted to examine the velocity profiles $f'(\eta)$, the temperature profiles $\theta(\eta)$ and the concentration fields $\phi(\eta)$, for expanding values of the viscosity parameter γ. The dependence of fluid viscosity on the temperature through the presence of γ invigorates both the fluid temperature $\theta(\eta)$ and the fluid concentration $\phi(\eta)$ distribution, while the presence of the γ parameter hinders the liquid velocity $f'(\eta)$ through the boundary layer. Physically, increasing the magnitude of the viscosity parameter acts as a retarding factor, causing the fluid velocity to slow down and, as a result, the friction between the fluid layers increases, causing the fluid temperature to enhance.

Figure 5 has been portrayed to delineate the impact of the thermal conductivity parameter ε. The larger values of the thermal conductivity parameter ε relate to the larger temperature distribution and marginal increments in the concentration field, while the growth in a same parameter makes insignificant decreases in the speed profiles. Physically, increasing the value of ε enhances the fluid thermal conductivity, which increases both the fluid temperature and the thickness of the thermal layer.

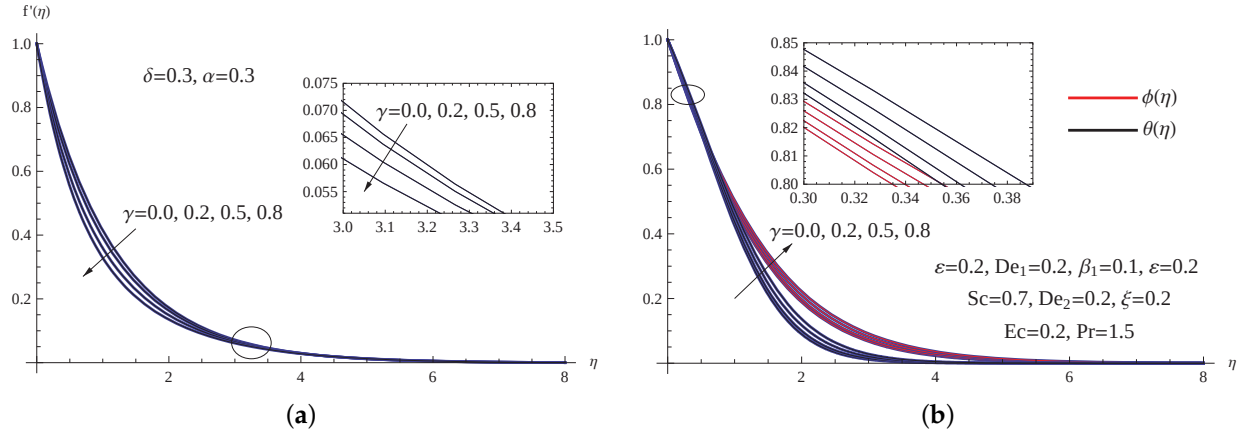

Figure 4. (**a**) $f'(\eta)$ for picked γ. (**b**) $\theta(\eta)$ and $\phi(\eta)$ for picked γ.

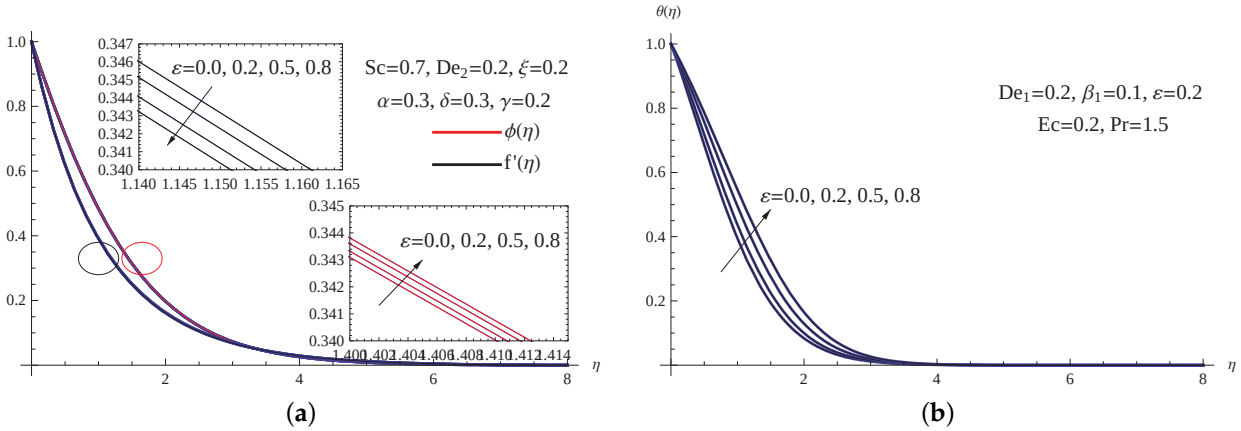

Figure 5. (**a**) $f'(\eta)$ and $\phi(\eta)$ for picked ε. (**b**) $\theta(\eta)$ for picked ε.

The actions of the velocity profiles $f'(\eta)$, the temperature profiles $\theta(\eta)$ and the concentration fields $\phi(\eta)$ for escalating values of the thermal Deborah number De_1 are depicted in Figure 6. The velocity distribution $f'(\eta)$ barely rises for the larger De_1 parameter, while the concentration profiles $\phi(\eta)$ are somewhat marginally decreased with the expansion of the same parameter De_1. In addition, expanded values of the same parameter De_1 lower both the temperature profiles and the thermal boundary thickness. In terms of physics, when the thermal Deborah number rises, the relaxation time for the heat flux also increases, meaning that both the thermal boundary layer thickness and the mechanism of heat diffusion become low.

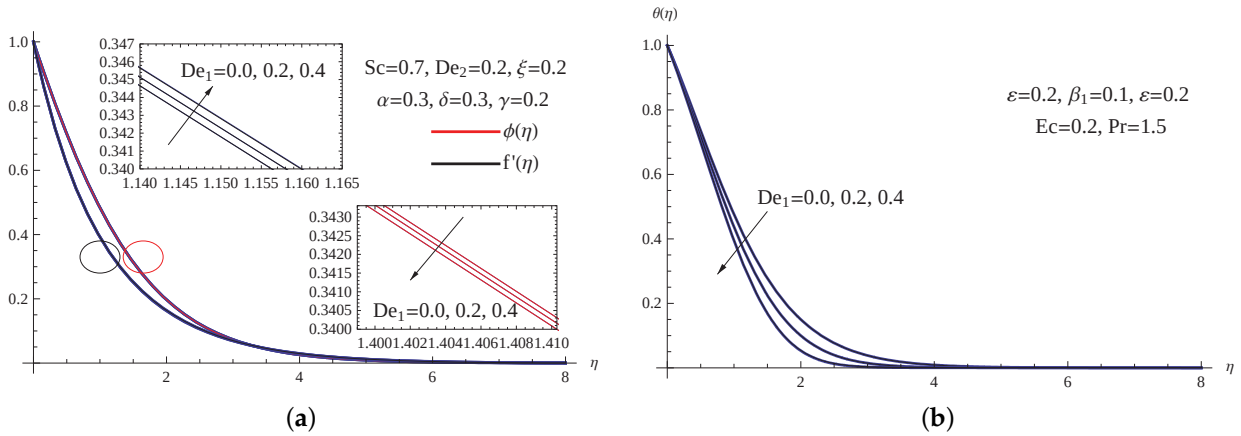

Figure 6. (**a**) $f'(\eta)$ and $\phi(\eta)$ for picked De_1. (**b**) $\theta(\eta)$ for picked De_1.

Figure 7 demonstrates the impact of the Eckert number Ec on the velocity $f'(\eta)$, thermal $\theta(\eta)$ and concentration $\phi(\eta)$ profiles. The upsurge in Eckert number Ec clearly works by improving both the thermal boundary thickness and the temperature profile. Further, a barely noticeable upgrade for the concentration profiles $\phi(\eta)$ is made due to the Eckert number Ec, while the inverse marginally noticeable pattern is noticed for the speed profile $f'(\eta)$. In physical terms, due to the dissipation phenomena, enhancing the value of Ec causes more heat energy to be created. This could explain why the temperature distribution within the thermal boundary layer is improving.

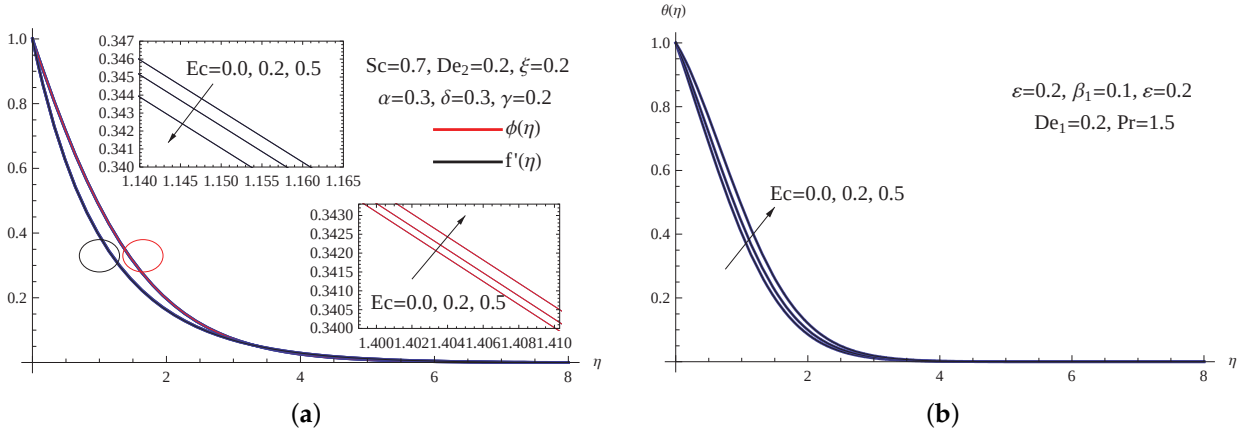

Figure 7. (**a**) $f'(\eta)$ and $\phi(\eta)$ for picked Ec. (**b**) $\theta(\eta)$ for picked Ec.

Finally, the endeavor to evoke the impact of both the Deborah number, which connected with the mass transfer De_2, and the chemical reaction parameter ξ on the mass transfer mechanism $\phi(\eta)$ has been made by drawing Figure 8. It is obvious that the increment in both parameters De_2 and ξ may help in creating an obstruction for the behavior of the fluid concentration mechanism $\phi(\eta)$. Physically, a higher De_2 indicates a longer period for the mass flux to relax. As a result, with greater De_2, the minimum mass diffusion rate occurs, lowering the fluid concentration.

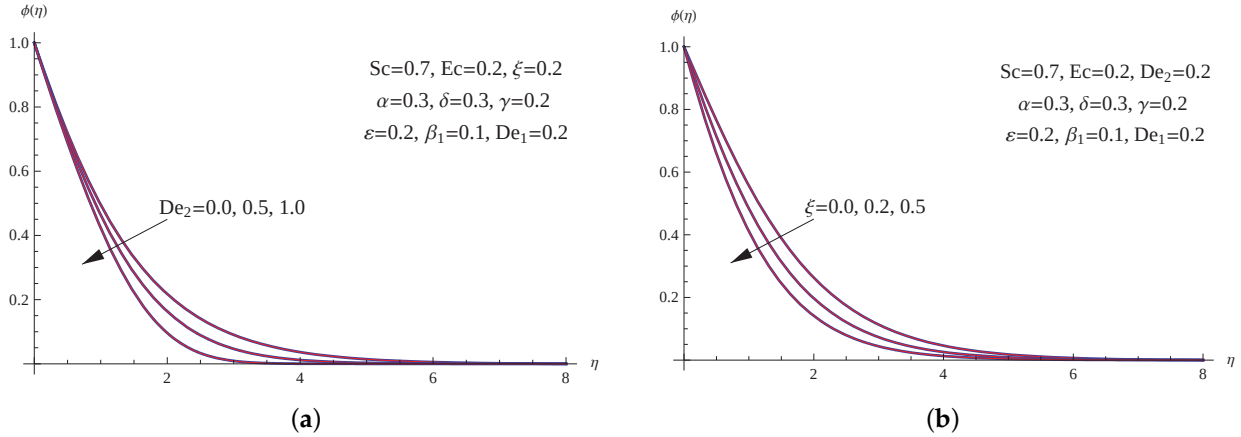

Figure 8. (**a**) $\phi(\eta)$ for picked De_2. (**b**) $\phi(\eta)$ for picked ξ.

The numerical outcomes for the local Nusselt number, the local Sherwood number, and the local skin-friction coefficient are displayed in Table 2 for different values of the arising parameters. From Table 2, it may be seen that because of an increment in the Powell–Eyring parameter α there is an expansion in the local skin-friction coefficient, the local Nusselt number, and the local Sherwood number, whereas the inverse pattern is noticed for the Powell–Eyring parameter δ. Additionally, from the same table, we note that the viscosity parameter decreases the local skin-friction coefficient, the local Nusselt

number, and the local Sherwood number. Further, Table 2 shows that the local skin-friction coefficient increments with expanding values of the thermal Deborah number, whereas it diminishes with the expanding values of the thermal conductivity parameter and the Eckert number. Furthermore, it is discernible that both the Eckert number and the chemical reaction parameter contribute to strengthening the local Sherwood number.

Table 2. Values for $Cf_x(Re_x)^{\frac{1}{2}}$, $Nu_x(Re_x)^{\frac{-1}{2}}$ and $Sh_x(Re_x)^{\frac{-1}{2}}$ for various values of α, δ, ε, γ, De_1, Ec, De_2 and ξ with $Pr = 1.5$ and $\beta_1 = 0.1$.

α	δ	γ	ε	De_1	Ec	De_2	ξ	$Cf_x(Re_x)^{\frac{1}{2}}$	$Nu_x(Re_x)^{\frac{-1}{2}}$	$Sh_x(Re_x)^{\frac{-1}{2}}$
0.0	0.3	0.2	0.2	0.2	0.2	0.2	0.2	0.920887	0.468142	0.599312
0.4	0.3	0.2	0.2	0.2	0.2	0.2	0.2	1.112051	0.502697	0.622836
0.6	0.3	0.2	0.2	0.2	0.2	0.2	0.2	1.197817	0.513244	0.631776
1.0	0.3	0.2	0.2	0.2	0.2	0.2	0.2	1.354441	0.527314	0.646012
0.3	0.0	0.2	0.2	0.2	0.2	0.2	0.2	1.074721	0.497792	0.618709
0.3	0.4	0.2	0.2	0.2	0.2	0.2	0.2	1.064221	0.495515	0.617431
0.3	0.6	0.2	0.2	0.2	0.2	0.2	0.2	1.058640	0.494284	0.616745
0.3	1.0	0.2	0.2	0.2	0.2	0.2	0.2	1.046602	0.491591	0.615261
0.3	0.3	0.0	0.2	0.2	0.2	0.2	0.2	1.134321	0.508799	0.625702
0.3	0.3	0.2	0.2	0.2	0.2	0.2	0.2	1.064230	0.496106	0.617760
0.3	0.3	0.5	0.2	0.2	0.2	0.2	0.2	0.973111	0.476591	0.606035
0.3	0.3	0.8	0.2	0.2	0.2	0.2	0.2	0.888698	0.456668	0.594712
0.3	0.3	0.2	0.0	0.2	0.2	0.2	0.2	1.068531	0.567536	0.617941
0.3	0.3	0.2	0.2	0.2	0.2	0.2	0.2	1.066933	0.496106	0.617760
0.3	0.3	0.2	0.5	0.2	0.2	0.2	0.2	1.064971	0.420572	0.617541
0.3	0.3	0.2	0.8	0.2	0.2	0.2	0.2	1.063412	0.366929	0.617372
0.3	0.3	0.2	0.2	0.0	0.2	0.2	0.2	1.065840	0.465177	0.617651
0.3	0.3	0.2	0.2	0.2	0.2	0.2	0.2	1.066933	0.496106	0.617760
0.3	0.3	0.2	0.2	0.4	0.2	0.2	0.2	1.068043	0.528122	0.617781
0.3	0.3	0.2	0.2	0.2	0.0	0.2	0.2	1.068581	0.609484	0.617951
0.3	0.3	0.2	0.2	0.2	0.2	0.2	0.2	1.066933	0.496106	0.617760
0.3	0.3	0.2	0.2	0.2	0.5	0.2	0.2	1.064471	0.326569	0.617477
0.3	0.3	0.2	0.2	0.2	0.2	0.0	0.2	1.066930	0.496106	0.609967
0.3	0.3	0.2	0.2	0.2	0.2	0.5	0.2	1.066930	0.496106	0.631066
0.3	0.3	0.2	0.2	0.2	0.2	1.0	0.2	1.066930	0.496106	0.658297
0.3	0.3	0.2	0.2	0.2	0.2	0.2	0.0	1.066930	0.496106	0.481006
0.3	0.3	0.2	0.2	0.2	0.2	0.2	0.2	1.066930	0.496106	0.617760
0.3	0.3	0.2	0.2	0.2	0.2	0.2	0.5	1.066930	0.496106	0.775697

6. Conclusions

In this research, we have examined the impact of the double diffusive Cattaneo–Christov phenomenon on the non-Newtonian Powell–Eyring fluid flow and heat mass transfer, together with viscous dissipation due to a stretching sheet. The controlling nonlinear equations were formed and tackled numerically by means of shooting technique. The acquired outcomes suggest the accompanying pronouncements.

1. The temperature distribution improves as the thermal conductivity parameter and the Eckert number improve, whereas the concentration distribution is affected by the chemical reaction parameter, which has a decreasing effect.
2. The higher the viscosity parameter, the slower the fluid velocity becomes, and the lower the thermal Deborah number, the higher the thermal distribution becomes.
3. The Nusselt number value diminishes for both higher values of thermal conductivity parameter and viscosity parameter.
4. There is an increase in the Sherwood number with an increment in the chemical reaction parameter or with a decline in the viscosity parameter.

5. The impact of diminishing the thermal Deborah number or expanding the thermal conductivity parameter reduces the speed profiles.
6. In the future, we intend to expand on this research by looking at chemically reactive mixed convective non-Newtonian fluid flows, as well as heat and mass fluxes, in order to control the cooling process.

Author Contributions: Conceptualization, K.M.K. and A.S.; methodology, A.M.M. and W.A.; software, A.M.M. and W.A.; validation, A.S. and K.M.K.; formal analysis, A.M.M. and W.A.; investigation, K.M.K.; resources, A.S.; writing—original draft preparation, A.M.M. and W.A.; writing—review and editing, K.M.K. and A.M.M.; visualization, W.A. All authors have read and agreed to the published version of the manuscript.

Funding: This research received no external funding.

Institutional Review Board Statement: Not applicable.

Informed Consent Statement: Not applicable.

Data Availability Statement: Not applicable.

Acknowledgments: The authors wish to express their sincere thanks to the honorable referees for their valuable comments and suggestions to improve the quality of the paper.

Conflicts of Interest: The authors declare no conflict of interest.

Nomenclature

a	velocity coefficient
c	Powell–Eyring parameter
c_p	specific heat at constant pressure
C	nanoparticles concentration
Cf_x	skin friction coefficient
C_w	surface nanoparticles concentration
C_∞	ambient nanoparticles concentration
De_1	thermal Deborah number
De_2	the mass Deborah number
Ec	Eckret number
f	dimensionless stream function
k_0	the rate of chemical reaction
Nu_x	local Nusselt number
Pr	Prandtl number
Q	heat generation (absorption) coefficient
Re_x	local Reynolds number
Sc	Schmidt number
T	fluid temperature
T_w	surface temperature
T_∞	ambient temperature
u	velocity component in the $x-$ direction
v	velocity component in the $y-$ direction
x, y	Cartesian coordinates
Greek symbols	
ρ	density of the fluid
μ	coefficient of viscosity
ν	kinematic viscosity
θ	dimensionless temperature
ϕ	dimensionless concentration
λ_1	relaxation time for heat flux
λ_2	relaxation time for mass flux

η	similarity variable
γ	viscosity parameter
ε	thermal conductivity parameter
ξ	chemical reaction parameter
β	Powell–Eyring parameter
β_1	the heat generation (absorption) parameter
κ	thermal conductivity
Superscripts	
$'$	differentiation with respect to η
∞	free stream condition
w	wall condition

References

1. Haliza, R.; Ishak, A.; Pop, I. Micropolar fluid flow towards a stretching/shrinking sheet in a porous medium with suction. *Int. Commun. Heat Mass Trans.* **2012**, *39*, 826–829.
2. Abel, M.S.; Tawade, J.V.; Nandeppanavar, M.M. MHD flow and heat transfer for the upper-convected Maxwell fluid over a stretching sheet. *Meccanica* **2012**, *47*, 385–393.
3. Megahed, A.M. Variable fluid properties and variable heat flux effects on the flow and heat transfer in a non-Newtonian Maxwell fluid over an unsteady stretching sheet with slip velocity. *Chin. Phys. B* **2013**, *22*, 484–489. [CrossRef]
4. Sun, X.; Wang, S.; Zhao, M. Numerical solution of oscillatory flow of Maxwell fluid in a rectangular straight duct. *Appl. Math. Mech.* **2019**, *40*, 1647–1656. [CrossRef]
5. Imran, M.A.; Sarwar, S.; Imran, M. Effects of slip on free convection flow of Casson fluid over an oscillating vertical plate. *Bound. Value Probl.* **2016**, *2016*, 30. [CrossRef]
6. Sharma, R.P.; Avinash, K.; Sandeep, N.; Makinde, O.D. Thermal radiation effect on non-Newtonian fluid flow over a stretched sheet of non-uniform thickness. *Defect Diffus. Forum* **2017**, *377*, 242–259. [CrossRef]
7. Muhammad, B.; Samia, A. Flow and heat transfer analysis of Eyring-Powell fluid over stratified sheet with mixed convection. *J. Egypt. Math. Soc.* **2020**, *28*, 40.
8. Megahed, A.M.; Abbas, W. Non-Newtonian Cross fluid flow through a porous medium with regard to the effect of chemical reaction and thermal stratification phenomenon. *Case Stud. Therm. Eng.* **2022**, *29*, 101715. [CrossRef]
9. Cattaneo, C. Sulla conduzione del calore. *Atti Semin. Mat. Fis. Univ. Modena Reggio Emilia* **1948**, *3*, 83–101.
10. Christov, C.I. On frame indifferent formulation of the Maxwell-Cattaneo model of finite-speed heat conduction. *Mech. Res. Commun.* **2009**, *36*, 481–486. [CrossRef]
11. Hayat, T.; Khan, M.I.; Farooq, M.; Alsaedi, A.; Waqas, M.; Yasmeen, T. Impact of Cattaneo-Christov heat flux model in flow of variable thermal conductivity fluid over a variable thicked surface. *Int. J. Heat Mass Trans.* **2016**, *99*, 702–710. [CrossRef]
12. Hayat, T.; Qayyum, S.; Shehzad, S.A.; Alsaedi, A. Chemical reaction and heat generation/absorption aspects in flow of Walters-B nanofluid with Cattaneo-Christov double-diffusion. *Results Phys.* **2017**, *7*, 4145–4152. [CrossRef]
13. Sui, J.; Zheng, L.; Zhang, X. Boundary layer heat and mass transfer with Cattaneo-Christov double-diffusion in upper-convective Maxwell nanofluid past a stretching sheet with slip velocity. *Int. J. Therm. Sci.* **2016**, *104*, 461–468. [CrossRef]
14. Shehzad, S.A.; Abbasi, F.M.; Hayat, T.; Ahmad, B. Cattaneo-Christov heat flux model for third-grade fluid flow towards exponentially stretching sheet. *Appl. Math. Mech.* **2016**, *37*, 761–768. [CrossRef]
15. Li, J.; Zheng, L.; Liu, L. MHD viscoelastic flow and heat transfer over a vertical stretching sheet with Cattaneo-Christov heat flux effects. *J. Mol. Liq.* **2016**, *221*, 19–25. [CrossRef]
16. Meraj, M.A.; Shehzad, S.A.; Hayat, T.; Abbasi, F.M.; Alsaedi, A. Darcy-Forchheimer flow of variable conductivity Jeffrey liquid with Cattaneo-Christov heat flux theory. *Appl. Math. Mech.* **2017**, *38*, 557–566. [CrossRef]
17. Shehzad, S.A.; Hayat, T.; Alsaedi, A.; Meraj, M.A. Cattaneo-Christov heat and mass flux model for 3D hydromagnetic flow of chemically reactive Maxwell liquid. *Appl. Math. Mech.* **2017**, *10*, 1347–1356. [CrossRef]
18. Prasad, K.V.; Vaidya, H.; Vajravelu, K.; Ramanjini, V. Analytical study of Cattaneo–Christov heat flux model for Williamson-nanofluid flow over a slender elastic sheet with variable thickness. *J. Nanofluids* **2018**, *7*, 583–594. [CrossRef]
19. Ullah, K.S.; Ali, N.; Hayat, T.; Abbas, Z. Heat transfer analysis based on Cattaneo–Christov heat flux model and convective boundary conditions for flow over an oscillatory stretching surface. *Therm. Sci.* **2019**, *23*, 443–455. [CrossRef]
20. Garia, R.; Rawat, S.K.; Kumar, M.; Yaseen, M. Hybrid nanofluid flow over two different geometries with Cattaneo–Christov heat flux model and heat generation: A model with correlation coefficient and probable error. *Chin. J. Phys.* **2021**, *74*, 421–439. [CrossRef]
21. Christopher, A.J.; Magesh, N.; Gowda, R.J.P.; Kumar, R.N.; Kumar, R.S.V. Hybrid nanofluid flow over a stretched cylinder with the impact of homogeneous–heterogeneous reactions and Cattaneo–Christov heat flux: Series solution and numerical simulation. *Heat Trans.* **2021**, *50*, 3800–3821. [CrossRef]

22. Abbaszadeh, M.; Dehghan, M.; Khodadadian, A.; Noii, N.; Heitzinger, C.; Wick, T. A reduced-order variational multiscale interpolating element free Galerkin technique based on proper orthogonal decomposition for solving Navier-Stokes equations coupled with a heat transfer equation: Nonstationary incompressible Boussinesq equations. *J. Comput. Phys.* **2021**, *426*, 109875. [CrossRef]
23. Parvizi, M.; Khodadadian, A.; Eslahchi, M.R. Analysis of Ciarlet-Raviart mixed finite element methods for solving damped Boussinesq equation. *J. Comput. Appl. Math.* **2020**, *379*, 112818. [CrossRef]
24. Rauf, A.; Abbas, Z.; Shehzad, S.A.; Alsaedi, A.; Hayat, T. Numerical simulation of chemically reactive Powell-Eyring liquid flow with double diffusive Cattaneo-Christov heat and mass flux theories. *Appl. Math. Mech.* **2018**, *39*, 467–476. [CrossRef]
25. Megahed, A.M.; Reddy, M.G.; Abbas, W. Modeling of MHD fluid flow over an unsteady stretching sheet with thermal radiation, variable fluid properties and heat flux. *Math. Comput. Simul.* **2021**, *185*, 583–593. [CrossRef]
26. Javed, T.; Ali, N.; Abbas, Z.; Sajid, M. Flow of an Eyring-Powellnon-Newtonian fluid over a stretching sheet. *Chem. Eng. Commun.* **2013**, *200*, 327–336. [CrossRef]